Research Square

Preprints are preliminary reports that have not undergone peer review.
They should not be considered conclusive, used to inform clinical practice,
or referenced by the media as validated information.

Matrix-Dependent Spreading and Metabolic Activity of Bovine Satellite Cell Myospheres in Three-Dimensional Culture

Chang Ge
McMaster University
Yunfeng Yuan
Fudan University
P. Ravi Selvaganapathy
McMaster University
Fei Geng
gengf@mcmaster.ca
McMaster University

Research Article

Keywords: 3D cell culture, bovine satellite cells, extracellular matrix, myosphere, matrix mechanics, muscle stem cells

Posted Date: November 11th, 2026

DOI: https://doi.org/10.21203/rs.3.rs-11437834/v1

License: This work is licensed under a Creative Commons Attribution 4.0 International License.
Read Full License

Additional Declarations: No competing interests reported.

RESEARCH ARTICLE

Matrix-Dependent Spreading and Metabolic Activity of Bovine Satellite Cell Myospheres in Three-Dimensional Culture

Chang Ge[1], Yunfeng Yuan[2], P. Ravi Selvaganapathy[1], Fei Geng[1,3*]

[1]School of Biomedical Engineering, McMaster University, Hamilton, Ontario, Canada
[2]Zhongshan Hospital, Fudan University, Shanghai, China
[3]W Booth School of Engineering Practice and Technology, McMaster University, Hamilton, Ontario, Canada

Running Title: ECM Effects on Bovine Myospheres in 3D

Email addresses:

Chang Ge: gec@mcmaster.ca

Yunfeng Yuan: yuan.yunfeng@zs-hospital.sh.cn

P. Ravi Selvaganapathy: selvaga@mcmaster.ca

Fei Geng: gengf@mcmaster.ca

*Corresponding author:

Fei Geng

Email: gengf@mcmaster.ca

Abstract

Three-dimensional culture provides a useful platform for examining how extracellular matrix (ECM) environments influence bovine satellite cell behavior. In this study, OPO-MOO-M17 bovine satellite cells were used to establish myosphere cultures and evaluate responses to Matrigel, collagen I, and LunaGel under conditions spanning nominal stiffness values from the pascal to kilopascal range. Myogenic differentiation capacity was first confirmed, and initial seeding density was evaluated to establish reproducible myosphere formation. Myosphere spreading and relative alamarBlue fluorescence were then quantified across the three matrix systems, while selected cell-state-associated markers were further examined in Matrigel cultures by immunofluorescence and quantitative reverse transcription polymerase chain reaction. Matrix encapsulation promoted peripheral outgrowth compared with non-encapsulated myospheres. In Matrigel, increasing matrix concentration was associated with greater spreading, whereas relative alamarBlue fluorescence increased at low and intermediate concentrations but decreased under the highest-concentration condition. Collagen I and LunaGel also produced matrix-dependent differences in spreading and relative metabolic activity, with the two readouts showing more similar directional responses within the tested conditions. In Matrigel, selected comparisons showed lower PAX7 and CDKN2A/p16INK4a transcript levels and higher MKI67 transcript levels relative to non-encapsulated controls. Overall, morphological spreading and relative metabolic activity did not consistently change in parallel across matrix conditions. These findings demonstrate that bovine satellite cell responses depend on the specific three-dimensional matrix environment and highlight the value of integrating morphological, metabolic, and cell-state-associated readouts when evaluating culture conditions.

Keywords: 3D cell culture; bovine satellite cells; extracellular matrix; myosphere; matrix mechanics; muscle stem cells

Introduction

Skeletal muscle satellite cells are resident muscle stem cells that contribute to muscle maintenance and regeneration through transitions between quiescence, activation, proliferation, and differentiation (Dumont et al. 2015). Their behavior is strongly influenced by the surrounding extracellular matrix (ECM), which provides both structural support and biochemical and mechanical cues that regulate cell adhesion, migration, proliferation, and maintenance of myogenic characteristics (Yin et al. 2013; Bonnans et al. 2014; Dzamba and DeSimone 2018; Zhang et al. 2021; Saraswathibhatla et al. 2023). Three-dimensional (3D) culture systems provide a useful platform for studying these cell–matrix interactions because they allow cells to interact with surrounding matrix components and neighboring cells in a spatially organized environment (Ravi et al. 2015; Nicolas et al. 2020).

An important challenge in evaluating 3D matrix environments is that matrix properties are interdependent. Changes in matrix concentration or crosslinking can alter not only stiffness, but also ligand availability, network architecture, transport, and susceptibility to cell-mediated remodeling (Zaman et al. 2006; Amirrah et al. 2022). Cellular responses therefore cannot necessarily be attributed to stiffness alone (Roca-Arroyo et al. 2025). In addition, visible myosphere spreading does not necessarily correspond to changes in cell number, metabolic activity, or cell-cycle state. Evaluation of 3D culture conditions therefore benefits from complementary morphological, metabolic, and molecular measurements.

Matrigel, collagen I, and gelatin-based hydrogels provide compositionally and mechanically distinct environments for 3D culture. Collagen I is a major structural component of skeletal muscle ECM and forms fibrillar networks that provide mechanical support and facilitate cell adhesion and matrix remodeling (Kjær 2004; Zhang et al. 2021; Hennessy and Simms 2023). Matrigel is a

basement-membrane-derived matrix containing laminin, collagen IV, and other bioactive ECM components (Passaniti et al. 2022), whereas LunaGel is a photocrosslinkable gelatin-based hydrogel whose properties can be modulated through crosslinking conditions (Pham et al. 2023). These materials therefore provide contrasting 3D environments in which matrix composition, preparation, and nominal mechanical properties vary simultaneously. Their effects are consequently best interpreted as matrix-dependent responses rather than isolated stiffness effects (Roca-Arroyo et al. 2025). Selected cell-state-associated markers can provide additional context: Pax7 is associated with satellite-cell identity, Ki67 with active cell cycling, and p16INK4a with senescence-associated states, although none of these markers alone defines a specific functional state (Olguín and Pisconti 2012; Sun and Kaufman 2018; Aguanno et al. 2019; Uxa et al. 2021; Safwan-Zaiter et al. 2022).

In this study, we compared Matrigel, collagen I, and LunaGel as 3D matrix environments for bovine satellite-cell myospheres. Myosphere formation and initial seeding density were first evaluated to establish a reproducible starting condition for subsequent matrix studies. Myosphere spreading and relative alamarBlue fluorescence were then assessed across the three matrix systems, while selected cell-state-associated markers were further examined in Matrigel cultures using immunofluorescence and quantitative reverse transcription polymerase chain reaction. We specifically examined whether morphological spreading and relative metabolic activity changed concordantly across matrix conditions and whether cell-state-associated markers provided complementary information beyond morphology alone. Together, these analyses provide a comparative framework for evaluating 3D matrix environments for bovine satellite-cell culture. The overall experimental workflow is summarized in Fig. 1.

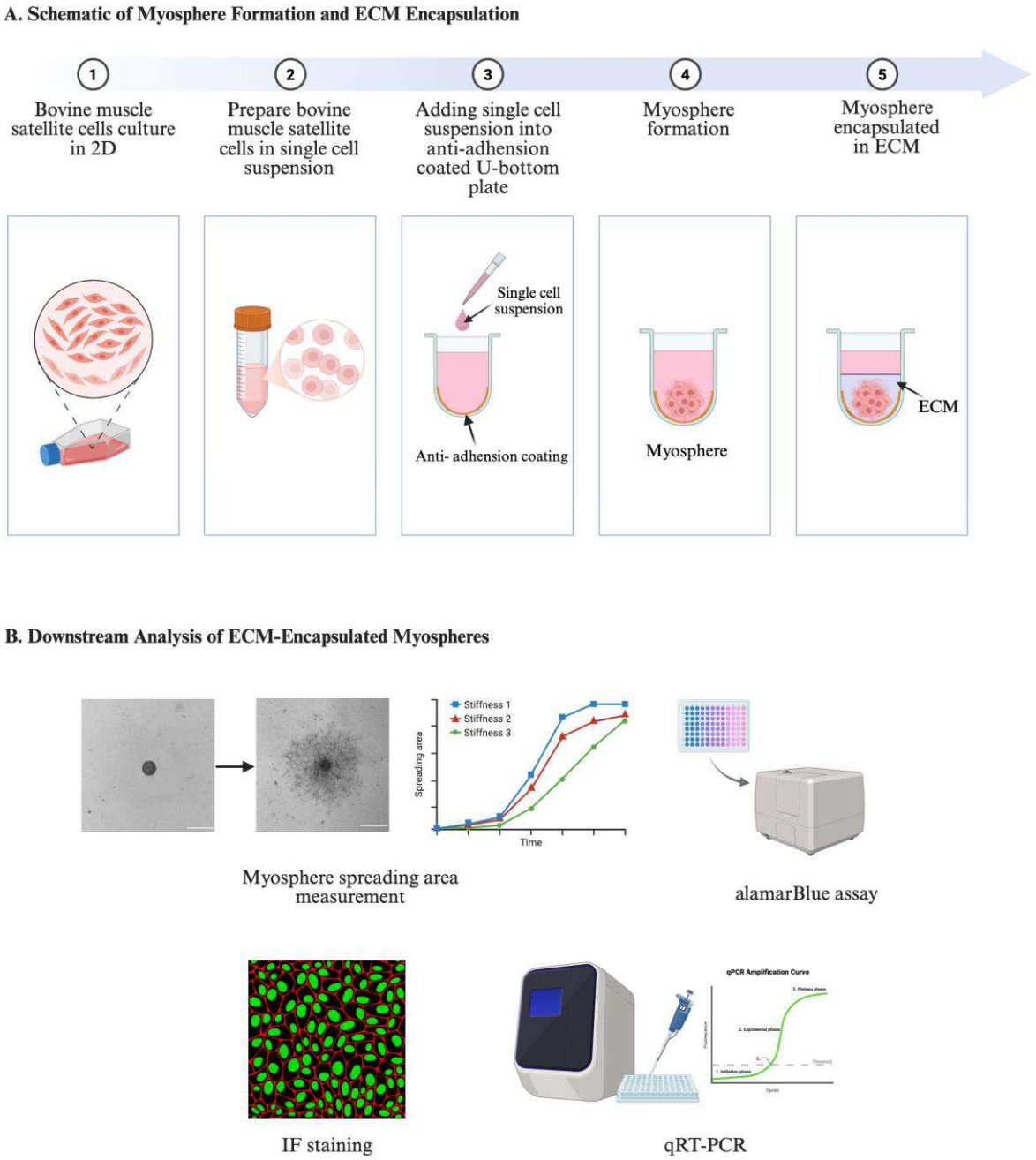


Fig. 1 Experimental workflow for bovine satellite cell myosphere formation, extracellular matrix encapsulation, and downstream analysis. (A) Schematic of the experimental workflow. OPO-MOO-M17 bovine satellite cells were expanded in two-dimensional culture, dissociated into a single-cell suspension, seeded into anti-adhesion-coated U-bottom plates, allowed to form myospheres, and subsequently encapsulated in extracellular matrix (ECM). (B) Overview of downstream analyses performed on ECM-encapsulated myospheres, including measurement of projected myosphere spreading area, alamarBlue assay for relative metabolic activity,

immunofluorescence staining, and quantitative reverse transcription polymerase chain reaction (qRT-PCR). The schematic was created using BioRender.

Materials and methods

Bovine satellite-cell culture

Primary bovine satellite cells (OPO-MOO-M17) were obtained from Opo Bio (New Zealand). Cells were maintained in Ham's F10 medium (Gibco) supplemented with 20% fetal bovine serum (FBS; Thermo Fisher Scientific), 0.625 μg/mL amphotericin B (Thermo Fisher Scientific), 100 U/mL penicillin–streptomycin (Thermo Fisher Scientific), and 5 ng/mL basic fibroblast growth factor (bFGF; Thermo Fisher Scientific). This formulation was used as the complete growth medium throughout the study. Cells were cultured at 37 °C in a humidified cell incubator containing 5% CO_2.

Myogenic differentiation

To induce myogenic differentiation, OPO-MOO-M17 cells were cultured in complete growth medium until they reached >80% confluence. Then the growth medium was replaced with differentiation medium consisting of DMEM (Thermo Fisher Scientific) supplemented with 2% horse serum (Gibco). Differentiation medium was replaced every 2 days.

Myosphere formation and seeding-density evaluation

Non-adherent culture plates were prepared by coating each well of a U-bottom 96-well plate (Sarstedt) with 60 μL of 0.02 g/mL poly(2-hydroxyethyl methacrylate) (poly-HEMA; Sigma-Aldrich). The plates were left in a biological safety cabinet for at least overnight until completely dry. Single-cell suspensions of OPO-MOO-M17 cells harvested from 2D cultures were then seeded into the coated wells in complete growth medium. To evaluate the effect of initial seeding

density on myosphere formation and size, cells were seeded at 1000, 2500, 4000, or 5000 cells/well, with three biological replicates per condition. Bright-field images were acquired using a BioTek Cytation 5 Cell Imaging Multimode Reader, beginning 3 h after seeding (day 0) and subsequently at 24-h intervals through day 4. Myosphere diameter was measured by drawing a line across each structure in ImageJ. For subsequent ECM encapsulation experiments, myospheres were generated using 2,500 cells/well and cultured for 48 h before encapsulation.

Matrix encapsulation

Myospheres were encapsulated in Matrigel, collagen I, or LunaGel 48 h after seeding.

Standard-concentration Matrigel (Corning, Cat. No. 354234) and high-concentration Matrigel (Corning, Cat. No. 354262) were used for myosphere encapsulation. For the initial experiment comparing Matrigel-encapsulated and non-encapsulated myospheres, Matrigel was prepared at a final concentration of 3.9 mg/mL, corresponding to a nominal stiffness of approximately 15 Pa. Subsequent concentration-dependent experiments used Matrigel at final concentrations of 1.56, 4.24, and 8.48 mg/mL, corresponding to nominal stiffness values of approximately 1.5, 21, and 90 Pa, respectively, based on manufacturer-reported concentration–storage modulus (G′) data. For encapsulation, part of the culture medium was removed from each well, leaving approximately 45 µL containing the myosphere. An equal volume of Matrigel prepared at twice the target concentration was added, yielding an approximately 90 µL encapsulation mixture at the desired concentration. Plates were incubated at 37 °C for 30–60 min to allow gelation, after which complete growth medium was added to bring the total volume to 200 µL per well.

Rat-tail collagen I (Thermo Fisher, Cat. No. A1048301) was prepared at 1 and 2.7 mg/mL using sterile 10× PBS, 1 M NaOH, and sterile water. Solutions were prepared on ice, and the pH was

adjusted to 7. These concentrations refer to the prepared collagen I solutions after neutralization. Reference stiffness values of approximately 5 and 50 Pa, respectively, were estimated from the concentration–storage modulus (G′) relationship (Motte and Kaufman 2013). Before encapsulation, most of the culture medium was carefully aspirated from the U-bottom wells without disturbing the myospheres. A 50 µL aliquot of the prepared collagen I solution was added directly to each well. Following polymerization at 37 °C for 30 min, 110 µL of complete growth medium was added to each well.

LunaGel (Gelomics, SKU0009) was prepared using the supplied photoinitiator. Each vial of lyophilized photoinitiator was reconstituted in 500 µL PBS, and the resulting 500 µL solution was mixed with 1 mL of the supplied ECM solution.

For LunaGel encapsulation, culture medium was removed as thoroughly as possible from the U-bottom wells while keeping the myospheres undisturbed. Subsequently, 50 µL of the ECM–photoinitiator mixture was added to each well. LunaGels were photocrosslinked using a LunaX Crosslinker (Gelomics) at a wavelength of 405 nm. Exposure times of 45 and 82 s were used, corresponding to manufacturer-reported nominal stiffness values of 7 and 12 kPa, respectively. Following the crosslinking, 50 µL of complete growth medium was added to each well.

Myosphere spreading analysis

Myosphere spreading was quantified from bright-field images acquired at 4× magnification using a BioTek Cytation 5 Cell Imaging Multimode Reader. Z-stack images were acquired using the instrument's software, with a step size of 2–20 µm selected according to sample size.

Images were imported into ImageJ and converted to 32-bit format. A threshold was applied to delineate the entire myosphere-associated structure, including the central myosphere and

surrounding cellular extensions, and its total projected area was measured. Percentage increase in projected area was calculated as $\frac{A_t - A_0}{A_0} \times 100$, where A_t represents the projected area at time t and A_0 represents the baseline projected area. Day 0 was used as the baseline for the initial Matrigel experiment, whereas Day 2 was used as the baseline for the subsequent Matrigel, collagen I, and LunaGel experiments. The projected area was used to assess myosphere spreading (Khaitan et al. 2006; Bianco et al. 2015; Kondapaneni et al. 2024). Data were compiled and analyzed using GraphPad Prism.

AlamarBlue assay

Metabolic activity was assessed using alamarBlue™ Cell Viability Reagent (Thermo Fisher), with fluorescence serving as an indirect measure of cellular reducing activity (Zachari et al. 2013). The volume of alamarBlue reagent added to each well was adjusted according to the existing culture volume, maintaining a reagent-to-culture-volume ratio of 1:10. Samples were then incubated at 37 °C for 16 h. Following incubation, the supernatant was transferred to a flat-bottom 96-well plate to reduce interference from the encapsulation material during fluorescence measurement. Fluorescence was measured using an Infinite M200 Pro microplate reader (Tecan, Männedorf, Switzerland). In a separate two-dimensional calibration experiment, alamarBlue fluorescence showed an approximately linear relationship with cell number over the tested range (Online Resource 1). For longitudinal comparisons, fluorescence values were normalized to the corresponding baseline measurement for each experimental condition. Data were compiled and analyzed using GraphPad Prism.

Immunofluorescence

Pax7 and Ki67 expression was examined by immunofluorescence staining. Matrigel-encapsulated myospheres were recovered using Cell Recovery Solution (Corning) and transferred to microcentrifuge tubes. Recovered myospheres were washed three times with PBS and fixed in 4% formaldehyde for 1 h at 4 °C with gentle agitation. Following six PBS washes, samples were permeabilized with 0.5% Triton X-100 in PBS for 2 h at room temperature and blocked overnight in 5% bovine serum albumin (BSA) in PBS at 4 °C with gentle agitation.

For Pax7 staining, myospheres were incubated overnight at 4 °C with a Pax7 primary antibody (1:10; Cat. No. PAX7; Developmental Studies Hybridoma Bank). Following six PBS washes, samples were incubated for 2 h at 4 °C with Alexa Fluor 488-conjugated goat anti-mouse IgG (H+L) cross-adsorbed secondary antibody (1:1,000; Cat. No. A-11001; Invitrogen).

For Ki67 staining, blocked myospheres were incubated overnight at 4 °C with a Ki67 primary antibody (1:200; Cat. No. ab15580; Abcam). Following six PBS washes, samples were incubated for 2 h at 4 °C with Alexa Fluor 647-conjugated donkey anti-rabbit IgG (H+L) highly cross-adsorbed secondary antibody (1:1,000; Cat. No. A-31573; Invitrogen). Primary and secondary antibody incubations were performed with gentle agitation.

Nuclei were stained with 4′,6-diamidino-2-phenylindole dihydrochloride (DAPI; 1:1,000; Thermo Fisher Scientific) for 40 min at room temperature. Samples were transferred to flat-bottom 96-well plates and imaged at 20× magnification using a BioTek Cytation 5 Cell Imaging Multimode Reader.

qRT-PCR

For RNA extraction from 3D cultures, non-encapsulated myospheres were washed three times with PBS and pelleted by centrifugation at 400 × g for 5 min at 4 °C. Matrigel-encapsulated

myospheres were recovered using Cell Recovery Solution (Corning). Following matrix dissolution, the recovered myospheres were transferred to microcentrifuge tubes, washed with PBS, and pelleted at 400 × g for 5 min at 4 °C.

Total RNA was extracted using the RNeasy Mini Kit (QIAGEN) and RNA concentration was measured using a BioTek Cytation 5 Cell Imaging Multimode Reader.

PAX7, MKI67, and CDKN2A/p16INK4a transcript levels were analyzed by quantitative reverse transcription polymerase chain reaction (qRT-PCR) using the iTaq Universal SYBR Green One-Step Kit (Bio-Rad), with GAPDH as the internal reference gene. Primer sequences are listed in Table 1. Relative gene expression was calculated using the $2^{-\Delta Ct}$ method, where $\Delta C_t = C_{t,target} - C_{t,GAPDH}$ (Schmittgen and Livak 2008). Data were compiled and analyzed using GraphPad Prism.

Gene	Forward	Reverse
GAPDH	5′-CACCCTCAAGATTGTCAGC-3′	5′-TAAGTCCCTCCACGATGC-3′
PAX7	5′-CTCCCTCTGAAGCGTAAGCA-3′	5′-GGTAGTGGGTCCTCTCGAA-3′
MKI67	5′-GAGACAGCCCAGGACACTTC-3′	5′-CCTGGTTCTCTGCACCATGT-3′
CDKN2A	5′-AGCTCGGACCTAAAGAAAGATTGA-3′	5′-GGACACCTGGGAAGAACTGG-3′

Table 1. Primer sequences used for qRT-PCR analysis. Primer sequences for target genes were designed and assessed for target specificity using Primer-BLAST. GAPDH was used as the internal reference gene for normalization.

Statistical analysis

Data are presented as mean ± standard deviation (SD). Differences between two groups were evaluated using unpaired, two-tailed Student's t-tests. For alamarBlue fluorescence measurements,

two-way ANOVA followed by Šídák's multiple-comparisons test was performed. A P value <0.05 was considered statistically significant. Unless otherwise specified, experiments were performed in triplicate. Statistical analyses were conducted using GraphPad Prism.

Results

Myogenic differentiation capacity of OPO-MOO-M17 bovine satellite cells

To confirm the myogenic differentiation capacity of OPO-MOO-M17 cells, cultures were switched to differentiation medium on Day 5 and monitored through Day 14 (Fig. 2A). Bright-field imaging showed progressive morphological changes following differentiation induction (Fig. 2B). Cells became increasingly elongated over time, with myotube-like structures becoming more evident at later time points. By Day 14, elongated and thickened structures were prominent throughout the culture.

To further characterize myogenic differentiation, cells at Day 14 were stained for F-actin and nuclei using phalloidin and DAPI, respectively (Fig. 2C). Immunofluorescence imaging showed elongated F-actin-positive structures containing multiple associated nuclei, consistent with multinucleated myotube-like morphology. These observations support the myogenic differentiation capacity of OPO-MOO-M17 cells under the tested culture conditions.

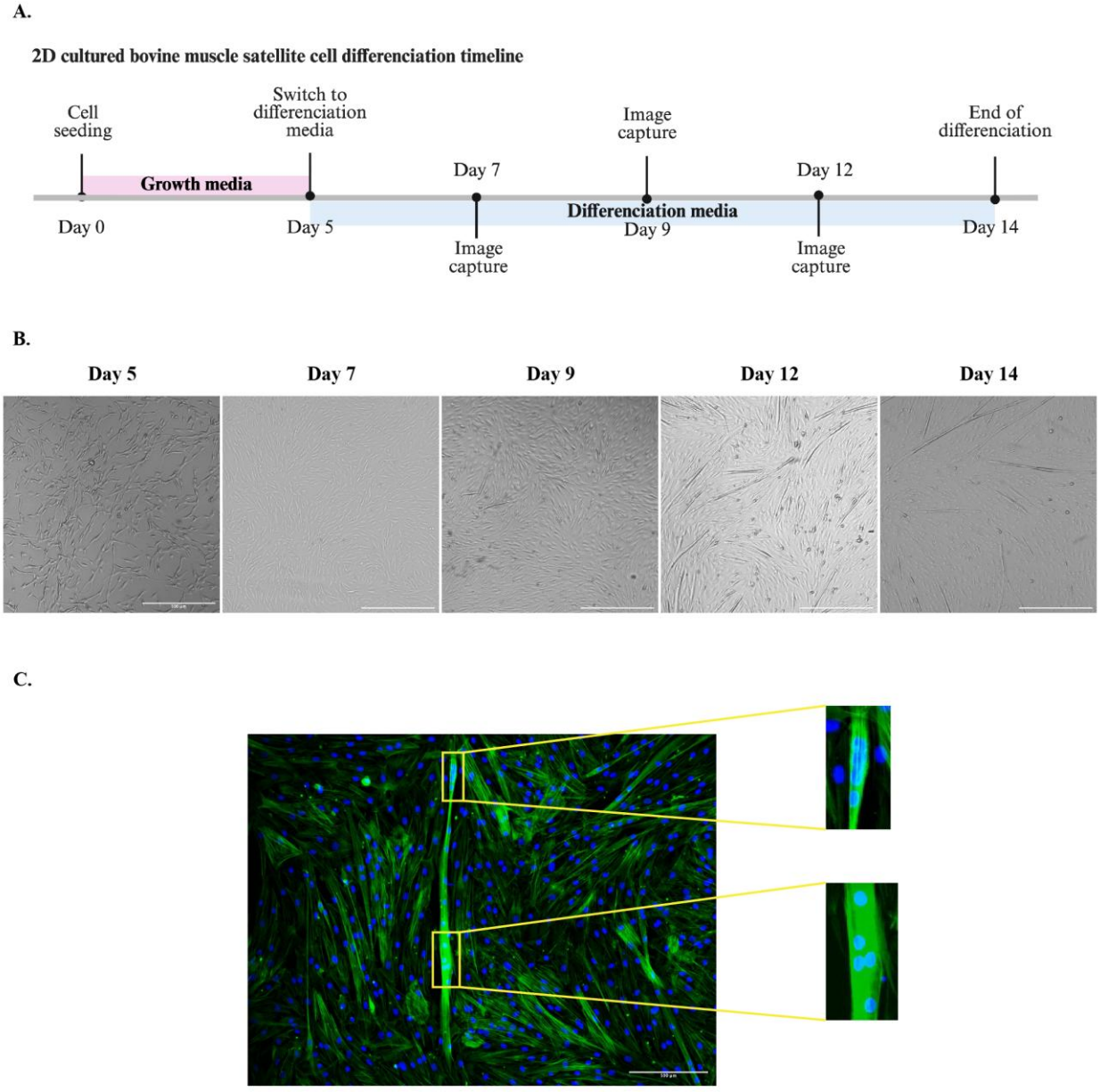


Fig. 2 Myogenic differentiation capacity of OPO-MOO-M17 bovine satellite cells. (A) Experimental timeline for two-dimensional myogenic differentiation. Cells were seeded on Day 0, maintained in growth medium through Day 5, and then switched to differentiation medium and cultured through Day 14. (B) Representative brightfield images acquired on Days 5, 7, 9, 12, and 14 showing progressive development of elongated myotube-like structures following differentiation induction. (C) Representative fluorescence image at Day 14 showing F-actin stained with phalloidin (green) and nuclei counterstained with DAPI (blue). Enlarged regions highlight elongated F-actin-positive structures containing multiple associated nuclei. Scale bars are shown in the images.

Seeding density influences bovine satellite cell myosphere formation and size

Bovine satellite cells were seeded into Poly-HEMA-coated, non-adherent U-bottom plates at initial densities of 1,000, 2,500, 4,000, and 5,000 cells per well to evaluate myosphere formation and size. Cells at all tested seeding densities self-assembled into compact myospheres under extracellular-matrix-free conditions. Representative brightfield images showed that myosphere size increased with increasing initial seeding density, while the overall spheroidal morphology was maintained during the four-day observation period (Fig. 3A).

Quantification of myosphere diameter showed a seeding-density-dependent pattern (Fig. 3B). Myospheres generated from higher initial cell numbers were consistently larger than those generated from lower seeding densities. For each seeding condition, myosphere diameter decreased modestly during the early culture period and subsequently remained relatively stable through Day 4. These results demonstrate that initial seeding density provides a reproducible means of controlling bovine satellite cell myosphere size under non-adherent culture conditions. The 2,500-cell-per-well condition was selected for the subsequent matrix-encapsulation experiments.

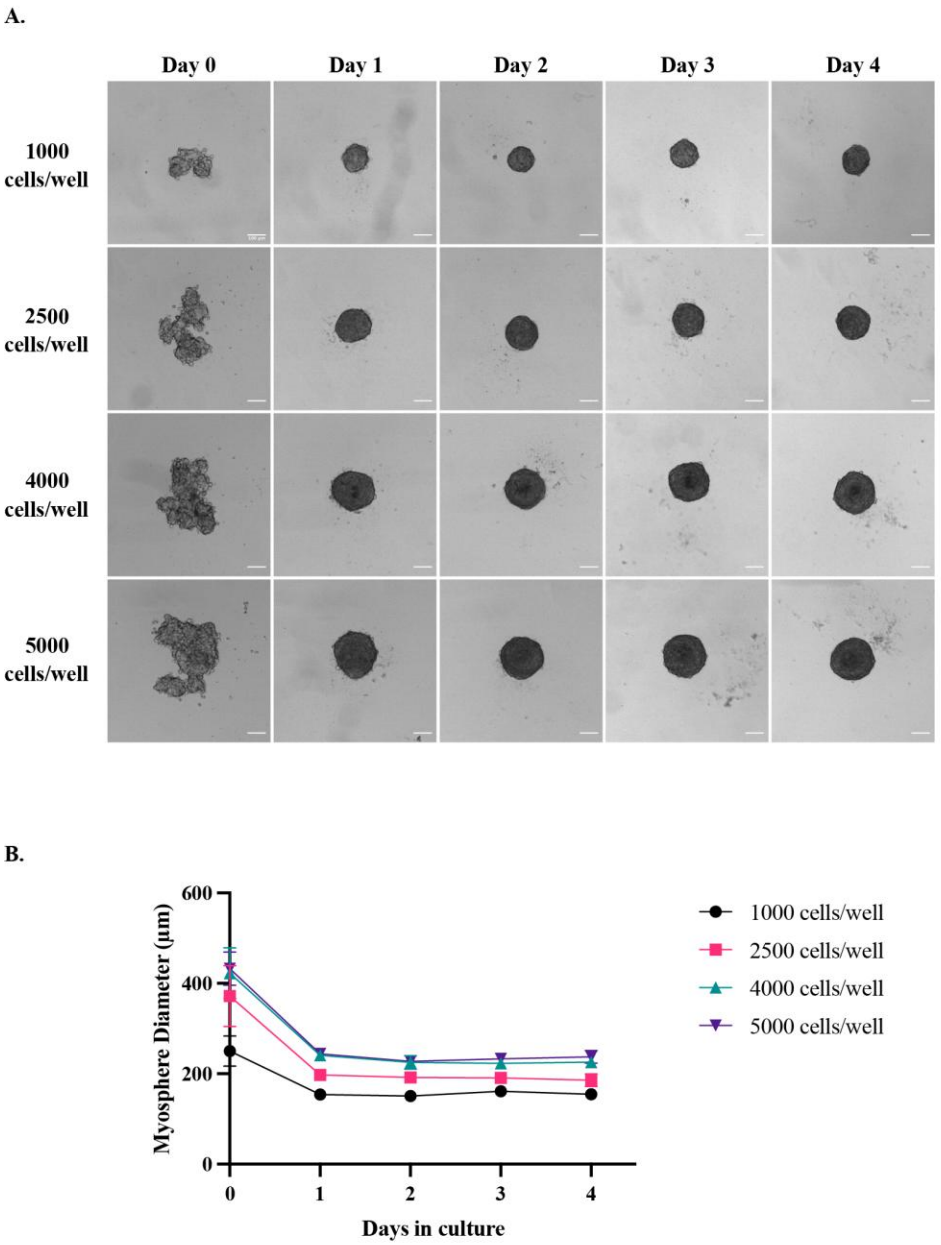


Fig. 3 Effect of initial seeding density on bovine satellite cell myosphere formation and size. (A) Representative brightfield images of myospheres generated using initial seeding densities of 1,000, 2,500, 4,000, and 5,000 cells/well and monitored from Day 0 through Day 4 under non-adherent, ECM-free culture conditions. Cells at all tested seeding densities formed compact myospheres, with larger initial cell numbers generally producing larger aggregates. (B) Quantification of myosphere diameter over the four-day culture period for each initial seeding density. Myosphere diameter decreased during the early aggregation period and subsequently remained relatively stable. Scale bars are shown in the images. Data are presented as mean ± SD (n = 3 independent experiments).

Matrigel encapsulation enhances myosphere spreading and relative metabolic activity

To determine whether incorporation of an extracellular matrix altered bovine satellite cell myosphere behavior, myospheres were cultured either without encapsulation or in Matrigel at 3.9 mg/mL, corresponding to a nominal stiffness of approximately 15 Pa. Non-encapsulated myospheres remained relatively compact during the four-day observation period, whereas Matrigel-encapsulated myospheres exhibited progressive peripheral outgrowth and expansion of the projected spreading area (Fig. 4A). Quantitative analysis showed an approximately 80% increase in projected myosphere area by Day 4 in the Matrigel condition, while substantially less spreading was observed in the non-encapsulated control (Fig. 4B).

Relative alamarBlue fluorescence also increased over the culture period in Matrigel-encapsulated myospheres, whereas the non-encapsulated controls showed comparatively little change (Fig. 4C). These results indicate that Matrigel encapsulation was associated with increased projected spreading and higher relative alamarBlue fluorescence under the tested condition. Based on these observations, subsequent experiments evaluated whether myosphere responses differed across a broader range of Matrigel concentrations and associated nominal mechanical conditions.

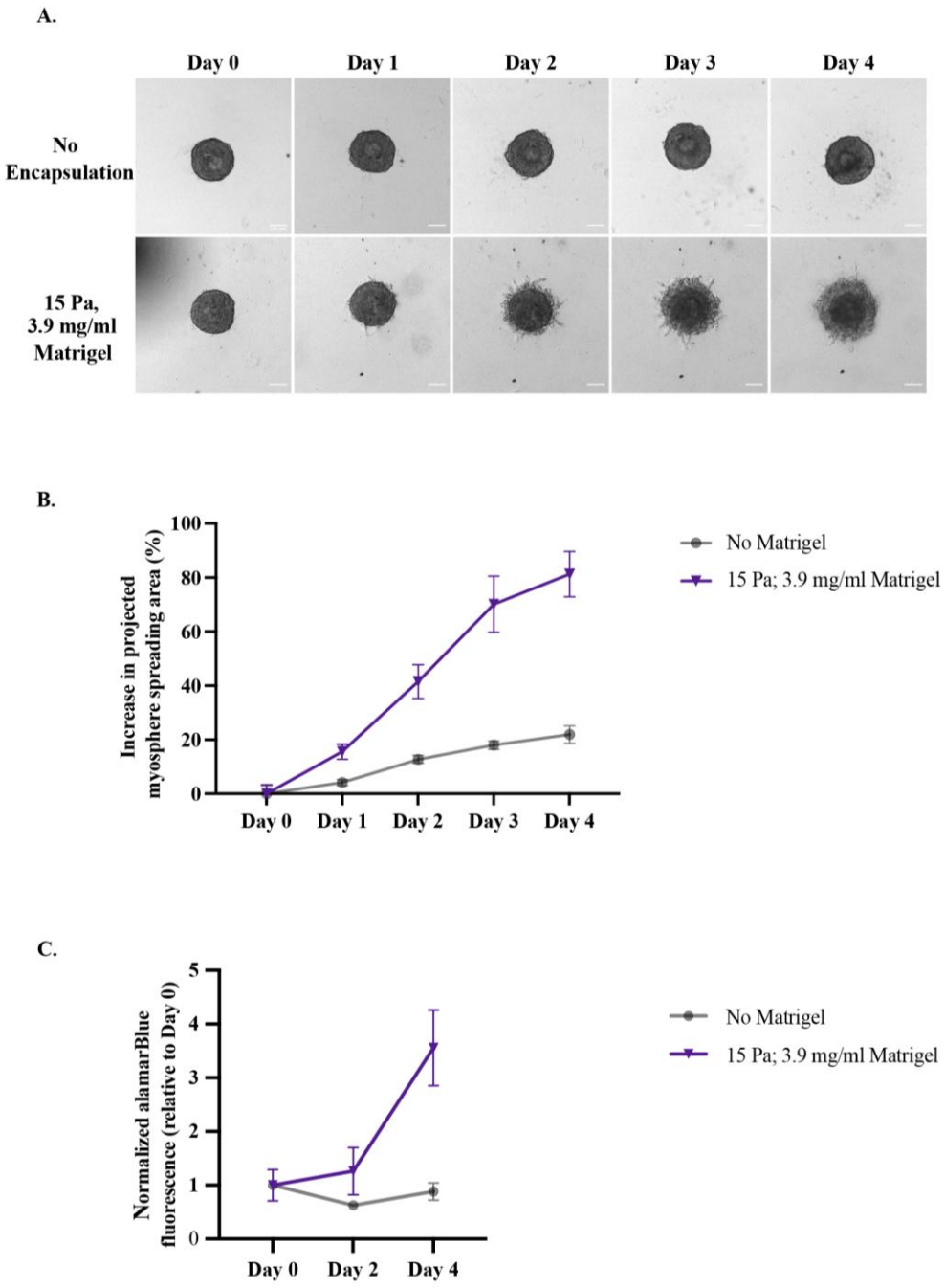


Fig. 4 Matrigel encapsulation enhances bovine satellite cell myosphere spreading and relative metabolic activity. (A) Representative brightfield images of non-encapsulated myospheres and myospheres encapsulated in 3.9 mg/mL Matrigel, corresponding to a nominal stiffness of approximately 15 Pa, from Day 0 through Day 4. The day of Matrigel encapsulation was defined as Day 0 for this experiment. (B) Quantification of myosphere spreading expressed as the percentage increase in projected myosphere area relative to Day 0. (C) Relative alamarBlue signal in non-encapsulated and Matrigel-encapsulated myospheres, normalized to the corresponding Day

0 value. Matrigel encapsulation was associated with increased myosphere spreading and relative metabolic activity during the observation period. Scale bars are shown in the images. Data are presented as mean ± SD (n = 3 independent experiments).

Matrigel concentration produces distinct spreading and metabolic responses

To examine whether bovine satellite cell myosphere responses varied with Matrigel concentration, myospheres were formed for 2 days before encapsulation and monitored through Day 10 (Fig. 5A). Myospheres were encapsulated in Matrigel at 1.56, 4.24, and 8.48 mg/mL, corresponding to nominal stiffness values of 1.5, 21, and 90 Pa, respectively. Following encapsulation, myospheres exhibited progressive peripheral outgrowth over the culture period, with greater projected spreading observed at higher Matrigel concentrations. The 8.48 mg/mL condition showed the most pronounced morphological expansion, whereas spreading was more limited at the lower Matrigel concentrations (Fig. 5B, C).

Relative alamarBlue fluorescence showed a different concentration-dependent pattern (Fig. 5D). Compared with the corresponding baseline measurement, the alamarBlue signal increased under the 1.56 and 4.24 mg/mL Matrigel conditions, whereas the 8.48 mg/mL condition showed a reduced signal at the final time point. Thus, the condition showing the greatest projected spreading did not show the greatest relative alamarBlue fluorescence.

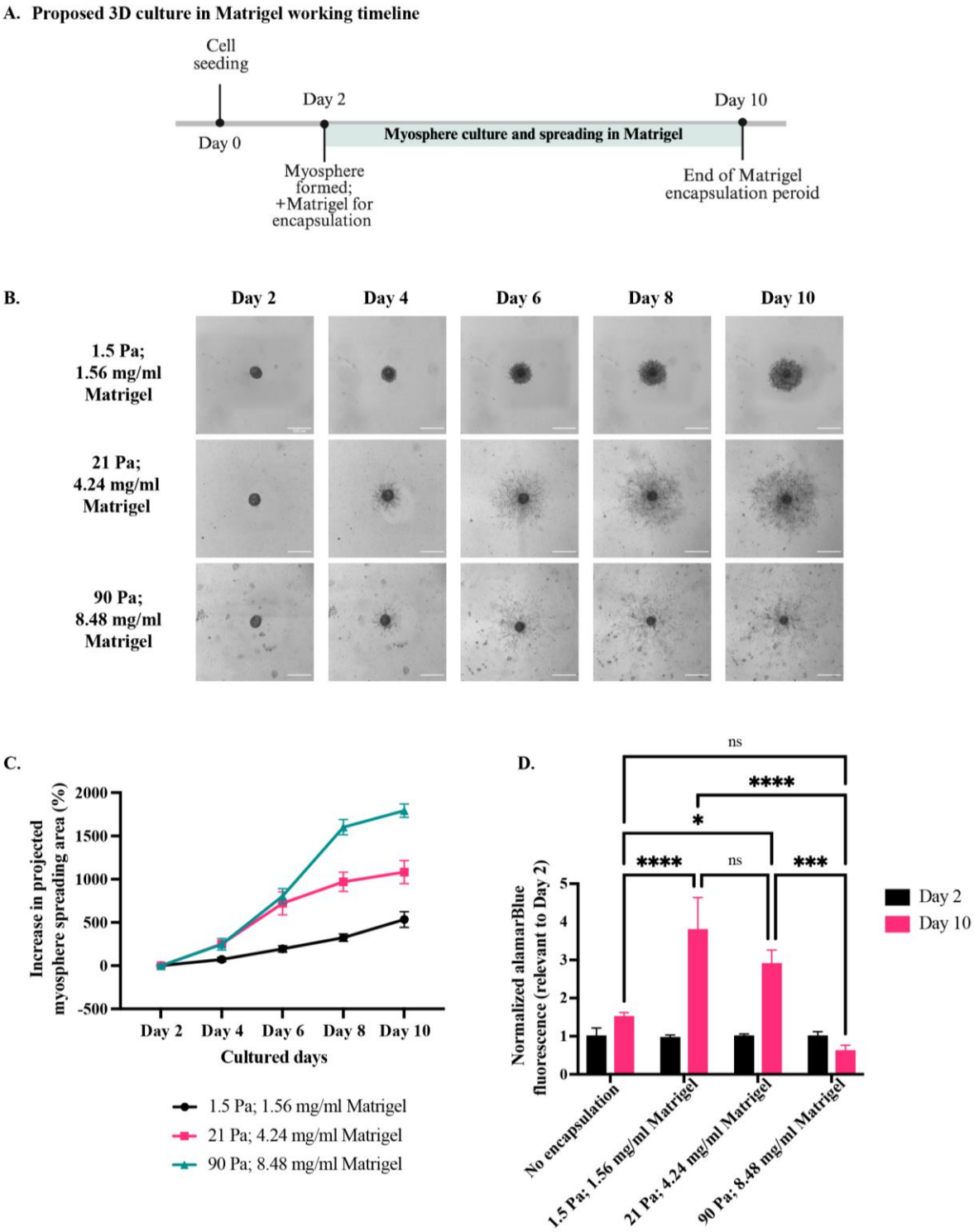


Fig. 5 Matrigel concentration produces distinct myosphere spreading and metabolic responses. (A) Experimental timeline for Matrigel-encapsulated myosphere culture. Cells were seeded on Day 0, myospheres were formed and encapsulated in Matrigel on Day 2, and cultures were monitored through Day 10. (B) Representative brightfield images of myospheres cultured in

1.56, 4.24, and 8.48 mg/mL Matrigel, corresponding to nominal stiffness values of 1.5, 21, and 90 Pa, respectively, from Day 2 through Day 10. (C) Quantification of projected myosphere spreading area over the culture period, expressed as the percentage increase relative to Day 2. (D) Relative alamarBlue fluorescence measured on Days 2 and 10 in non-encapsulated controls and the three Matrigel conditions and normalized to the corresponding Day 2 value. Higher Matrigel concentrations were associated with greater morphological spreading, whereas relative metabolic activity showed a different concentration-dependent pattern. Scale bars are shown in the images. Data are presented as mean ± SD (n = 3 independent experiments). Brackets indicate the statistical comparisons shown; ns, not significant; *$p < 0.05$, ***$p < 0.001$, and ****$p < 0.0001$.

Matrigel conditions are associated with distinct cell-state marker profiles

To further characterize cellular responses to Matrigel encapsulation, Pax7 and Ki67 expression was examined by immunofluorescence in non-encapsulated myospheres and in myospheres cultured under the 1.5, 21, and 90 Pa nominal Matrigel conditions. Representative images showed more prominent Pax7 staining in non-encapsulated myospheres, whereas Ki67 staining was evident in the 1.5 and 21 Pa conditions. In contrast, Ki67 staining appeared relatively sparse under the 90 Pa condition despite the pronounced morphological spreading observed at this Matrigel concentration (Fig. 6A). These observations indicate that the extent of myosphere spreading was not consistently accompanied by corresponding changes in cell-cycle-associated staining across the tested Matrigel conditions.

To complement the immunofluorescence analysis, qRT-PCR was performed to compare non-encapsulated myospheres with myospheres cultured in 4.24 mg/mL Matrigel, corresponding to a nominal stiffness of 21 Pa. Relative to the non-encapsulated control, Matrigel-encapsulated myospheres showed lower PAX7 and CDKN2A/p16INK4a transcript levels and higher MKI67 transcript levels (Fig. 6B). Together, these findings demonstrate that Matrigel encapsulation was associated with changes in selected markers related to satellite cell identity and cell-cycle state.

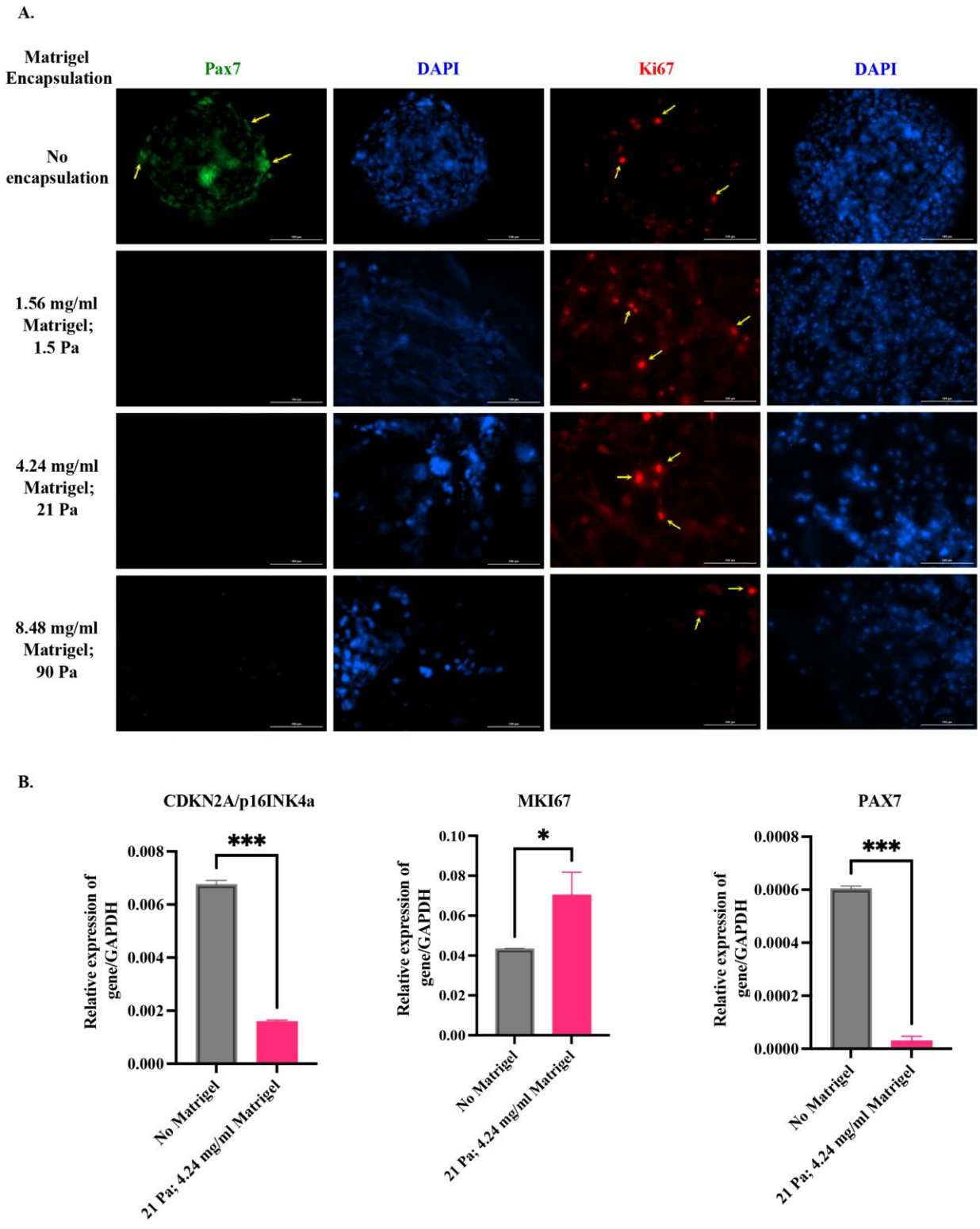


Fig. 6 Cell-state-associated marker profiles in non-encapsulated and Matrigel-encapsulated bovine satellite cell myospheres. (A) Representative immunofluorescence images of Pax7

(green) and Ki67 (red) in non-encapsulated myospheres and myospheres cultured in Matrigel at 1.56, 4.24, and 8.48 mg/mL, corresponding to nominal stiffness values of 1.5, 21, and 90 Pa, respectively. Nuclei were counterstained with DAPI (blue). Arrows indicate representative Pax7- or Ki67-positive staining. Scale bars are shown in the images. (B) qRT-PCR analysis of CDKN2A/p16INK4a, MKI67, and PAX7 transcript levels in non-encapsulated myospheres and myospheres cultured in 4.24 mg/mL Matrigel (21 Pa nominal stiffness). Transcript levels were normalized to GAPDH. Data are presented as mean ± SD (n = 3). Statistical comparisons were performed as described in the Methods; *$p < 0.05$ and ***$p < 0.001$.

Collagen I concentration influences myosphere spreading and metabolic activity

To determine whether myosphere responses also varied across collagen I conditions, myospheres were formed for 2 days before encapsulation and monitored through Day 10 (Fig. 7A). Myospheres were cultured without encapsulation or encapsulated using collagen I solutions prepared at concentrations of 1.0 and 2.7 mg/mL, with corresponding reference stiffness values of approximately 5 and 50 Pa. Non-encapsulated myospheres remained relatively compact throughout the culture period, whereas collagen I-encapsulated myospheres exhibited progressive peripheral outgrowth. Quantification of projected area showed greater spreading in the collagen I conditions, with the 2.7 mg/mL condition exhibiting the most pronounced increase by Day 10 (Fig. 7B, C).

Relative alamarBlue fluorescence also increased over the culture period in collagen I-encapsulated myospheres, with the greatest Day 10 response observed in the 2.7 mg/mL condition (Fig. 7D). Within the tested collagen I conditions, the higher-concentration condition therefore showed both greater projected spreading and higher relative alamarBlue fluorescence (Fig. 7C, D).

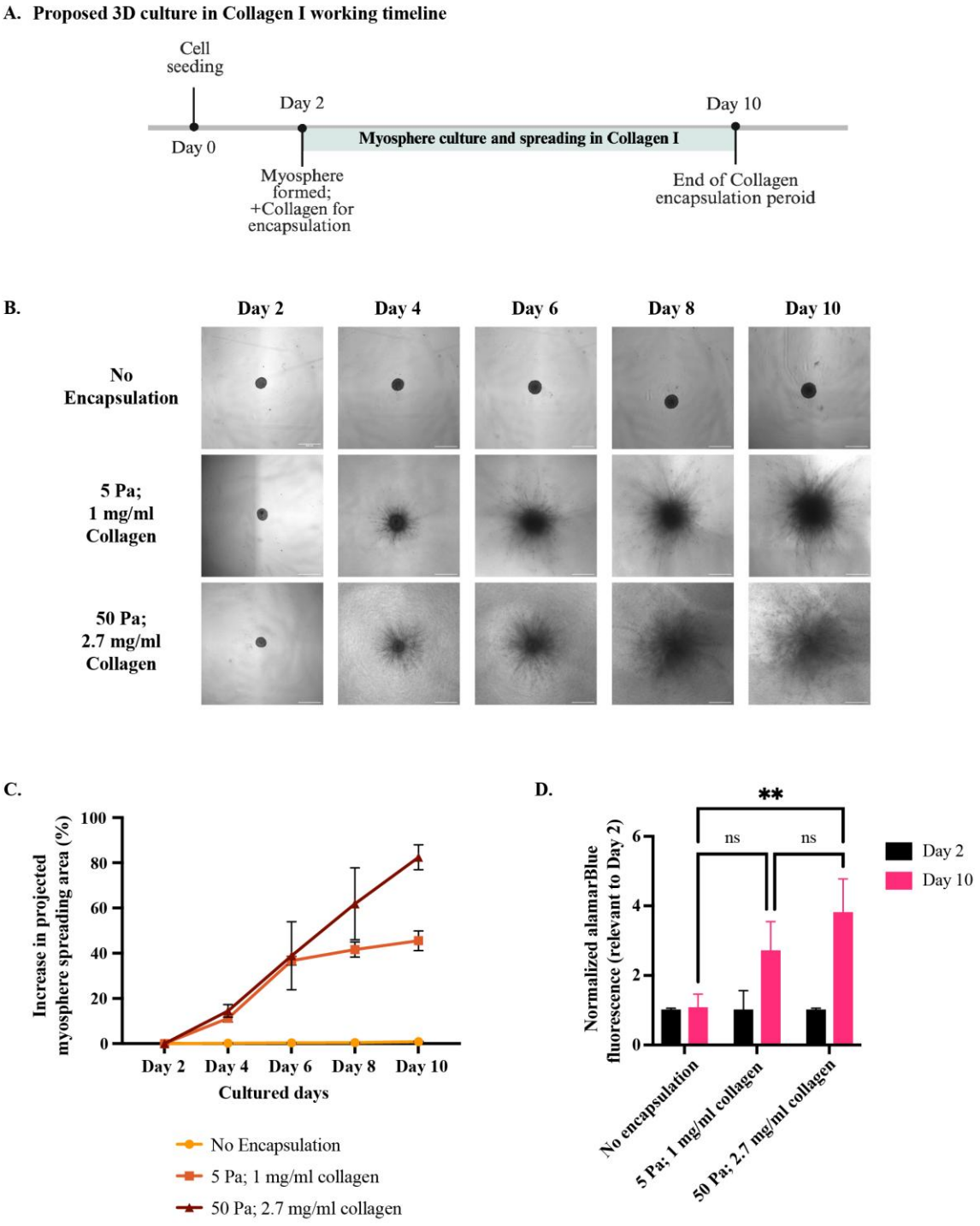


Fig. 7 Collagen I concentration influences bovine satellite cell myosphere spreading and relative metabolic activity. (A) Experimental timeline for collagen I-encapsulated myosphere culture. Cells were seeded on Day 0, myospheres were formed and encapsulated on Day 2, and cultures were monitored through Day 10. (B) Representative brightfield images of non-

encapsulated myospheres and myospheres encapsulated in collagen I at 1.0 and 2.7 mg/mL, corresponding to nominal stiffness values of approximately 5 and 50 Pa, respectively, from Day 2 through Day 10. (C) Quantification of projected myosphere spreading area over the culture period, expressed as the percentage increase relative to Day 2. (D) Relative alamarBlue fluorescence measured on Days 2 and 10 and normalized to the corresponding Day 2 value. Scale bars are shown in the images. Data are presented as mean ± SD (n = 3 independent experiments). Brackets indicate the statistical comparisons shown; ns, not significant; **$p < 0.01$.

LunaGel crosslinking conditions influence myosphere spreading and metabolic activity

To evaluate myosphere responses in a photocrosslinkable gelatin-based matrix, myospheres were formed for 2 days before encapsulation and monitored through Day 10 (Fig. 8A). Myospheres were cultured without encapsulation or in LunaGel under conditions corresponding to nominal stiffness values of 7 and 12 kPa. Non-encapsulated myospheres remained relatively compact, whereas LunaGel-encapsulated myospheres exhibited progressive peripheral outgrowth over the culture period. Quantification of projected area showed greater spreading under both LunaGel conditions, with the 12 kPa condition exhibiting the most pronounced increase by Day 10 (Fig. 8B, C).

Relative alamarBlue fluorescence also varied across the tested conditions. At Day 10, both LunaGel conditions showed higher relative alamarBlue fluorescence than the non-encapsulated control, whereas the difference between the 7 and 12 kPa conditions was not statistically significant (Fig. 8D). Although the 12 kPa condition showed the greatest projected spreading (Fig. 8C), this was not accompanied by a significantly greater alamarBlue response than the 7 kPa condition.

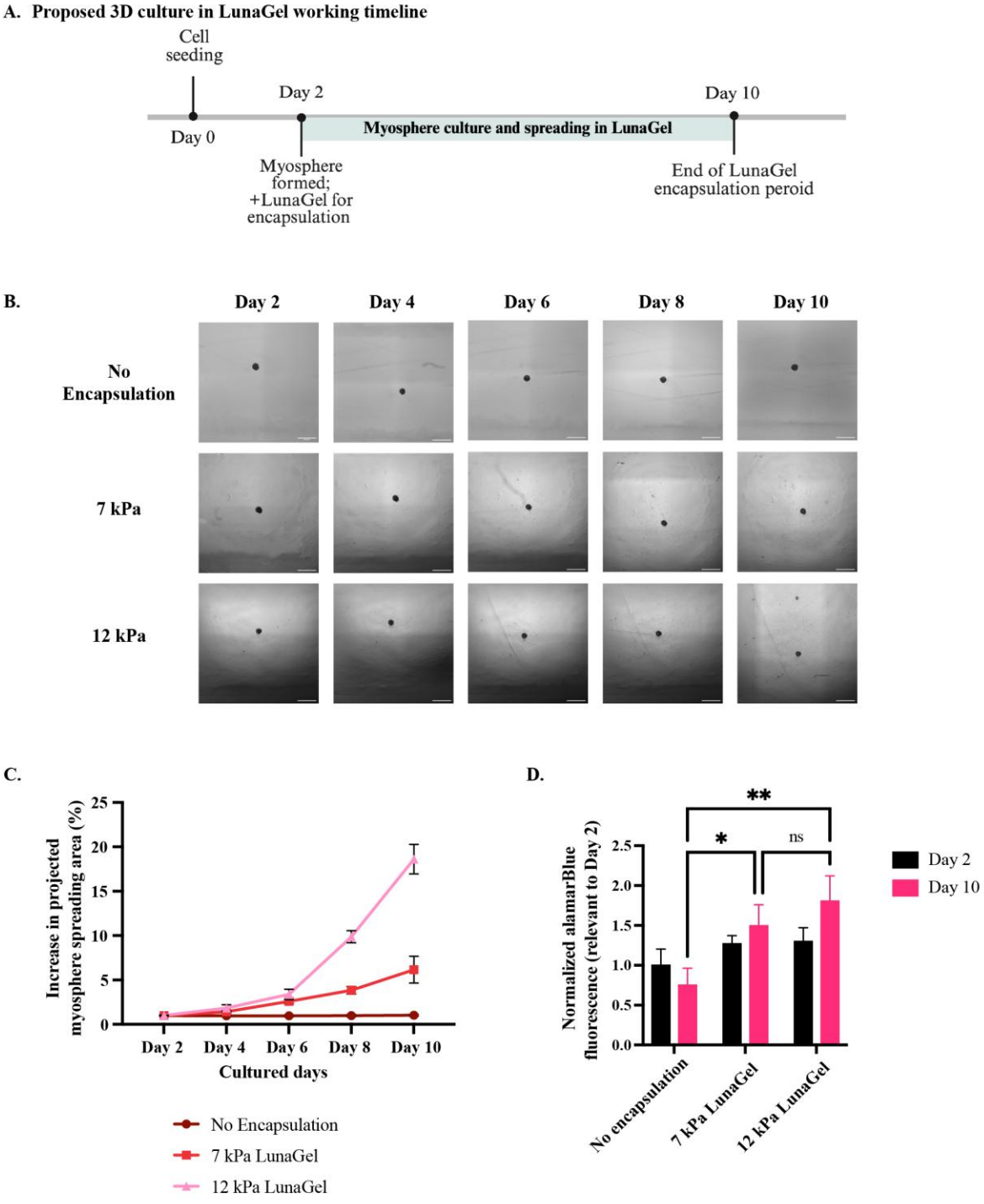


Fig. 8 LunaGel crosslinking conditions influence bovine satellite cell myosphere spreading and relative metabolic activity. (A) Experimental timeline for LunaGel-encapsulated myosphere culture. Cells were seeded on Day 0, myospheres were formed and encapsulated on Day 2, and cultures were monitored through Day 10. (B) Representative brightfield images of non-

encapsulated myospheres and myospheres cultured in LunaGel under conditions corresponding to nominal stiffness values of 7 and 12 kPa from Day 2 through Day 10. (C) Quantification of projected myosphere spreading area over the culture period, expressed as the percentage increase relative to Day 2. (D) Relative alamarBlue fluorescence measured on Days 2 and 10 and normalized to the corresponding Day 2 value. Scale bars are shown in the images. Data are presented as mean ± SD (n = 3 independent experiments). Brackets indicate the statistical comparisons shown; ns, not significant; *$p < 0.05$ and **$p < 0.01$.

Discussion

This study compared three-dimensional matrix environments for bovine satellite cell myospheres using complementary morphological, metabolic, and cell-state-associated readouts. OPO-MOO-M17 cells retained myogenic differentiation capacity (Fig. 2) and reproducibly formed compact myospheres under non-adherent conditions, with initial seeding density providing a practical means of controlling aggregate size (Fig. 3A, B). Across the matrix experiments, the central finding was that myosphere spreading and relative metabolic activity did not necessarily change in parallel. This divergence was most apparent in Matrigel, where the highest-concentration condition produced the greatest spreading but not the greatest alamarBlue response (Fig. 5C, D). These findings demonstrate that visible outgrowth alone is insufficient for evaluating cellular responses to three-dimensional matrix environments.

Matrigel produced the clearest separation between morphological and metabolic responses. Initial encapsulation in 3.9 mg/mL Matrigel increased both spreading and relative alamarBlue fluorescence compared with non-encapsulated myospheres (Fig. 4A–C). However, across the broader concentration range, increasing Matrigel concentration was associated with progressively greater spreading (Fig. 5B, C), whereas relative alamarBlue fluorescence increased at low and intermediate concentrations but declined at the highest concentration (Fig. 5D). Thus, extensive morphological outgrowth did not necessarily correspond to increased cellular reducing activity, while viable cell number was not independently measured. Changes in Matrigel concentration can

simultaneously affect matrix mechanics, ligand availability, network architecture, transport, and cell-mediated remodeling, making it difficult to attribute these responses to stiffness alone (Zaman et al. 2006; Amirrah et al. 2022). Previous studies have similarly shown that extracellular mechanics influence muscle stem and progenitor cell behavior (Gilbert et al. 2010; Van Santen et al. 2022), but the present results emphasize that three-dimensional matrix responses should be interpreted in the context of the complete matrix environment rather than nominal stiffness alone.

The Matrigel marker analyses provided additional context for this divergence. Representative immunofluorescence images showed Ki67 staining under the 1.5 and 21 Pa nominal conditions but relatively sparse staining under the 90 Pa condition despite extensive spreading (Fig. 6A). In the 4.24 mg/mL Matrigel condition, qRT-PCR showed higher MKI67 and lower PAX7 and CDKN2A/p16INK4a transcript levels relative to non-encapsulated controls (Fig. 6B). These changes are consistent with altered cell-cycle- and myogenic-state-associated responses, but they do not independently establish functional states such as release from quiescence, reversal of senescence, or preservation of long-term satellite cell potential. The marker data therefore reinforce the value of interpreting morphology together with metabolic and molecular measurements.

Collagen I and LunaGel showed a somewhat different pattern. Within the tested collagen I conditions, the higher-concentration condition showed greater spreading (Fig. 7B, C) together with a larger relative alamarBlue response (Fig. 7D). Similarly, the 12 kPa LunaGel condition showed greater spreading than the 7 kPa condition (Fig. 8B, C), whereas relative alamarBlue fluorescence did not differ significantly between the two LunaGel conditions at the final time point (Fig. 8D). These findings indicate that the relationship between morphology and metabolic activity is matrix dependent. However, collagen I, Matrigel, and LunaGel differ substantially in biochemical

composition, network structure, preparation method, and nominal mechanical properties, and they were not evaluated at matched stiffness values. The results should therefore be interpreted as comparisons among distinct three-dimensional culture environments rather than as evidence for a universal stiffness–response relationship.

Taken together, the three matrix systems produced distinct relationships between myosphere spreading and relative metabolic activity (Figs. 5, 7, and 8). The clearest divergence occurred in Matrigel, where the highest-concentration condition produced extensive spreading but a reduced relative alamarBlue response and relatively sparse Ki67 staining (Figs. 5C, D and 6A). In contrast, spreading and metabolic activity showed more similar directional responses within the tested collagen I and LunaGel conditions (Figs. 7C, D and 8C, D). These findings indicate that visible outgrowth alone may not adequately reflect cellular activity and support the use of complementary morphological, metabolic, and molecular readouts when evaluating 3D matrix environments.

Several limitations should be considered. Matrix concentration and crosslinking varied together with nominal mechanical properties, and matrix stiffness was not measured directly under the specific culture conditions used here. Consequently, the effects of stiffness cannot be separated from differences in matrix composition, ligand availability, network architecture, transport, or remodeling. In addition, alamarBlue fluorescence provides an indirect measure of cellular reducing activity and does not independently establish viable cell number. Molecular analyses were restricted to selected Matrigel conditions, and long-term expansion, quantitative cell recovery, post-recovery viability, maintenance of differentiation capacity, and performance under scalable culture conditions were not evaluated.

Conclusion

Bovine satellite cell myospheres showed distinct responses across three-dimensional matrix environments. The clearest divergence occurred in Matrigel, where the highest-concentration condition produced the greatest spreading but not the greatest relative alamarBlue response. The 4.24 mg/mL Matrigel condition was also associated with higher MKI67 and lower PAX7 and CDKN2A/p16INK4a transcript levels relative to non-encapsulated controls. In contrast, collagen I and LunaGel showed more similar directional relationships between spreading and metabolic activity. These findings support evaluating 3D matrices using complementary morphological, metabolic, and molecular readouts rather than nominal stiffness alone.

Acknowledgements Not applicable.

Author contributions C.G. performed the experiments, analyzed the data, prepared the figures, and contributed to manuscript preparation. Y.Y. contributed to data interpretation and manuscript review and revision. P.R.S. contributed to study design and manuscript review and revision. F.G. conceived and supervised the study, secured funding, contributed to data interpretation, and revised the manuscript. All authors reviewed and approved the final manuscript.

Funding This work was supported by Genome Canada through the Climate-Smart Agriculture and Food Systems (CSAFS) initiative.

Data availability The datasets generated and/or analyzed during the current study are available from the corresponding author upon reasonable request.

Declarations

Ethics approval Not applicable. The study was conducted using commercially obtained bovine satellite cells and did not involve human participants or the direct use of live animals.

Consent for publication Not applicable.

Competing interests The authors declare no competing interests.

References

Aguanno S, Petrelli C, Di Siena S, et al (2019) A Three-Dimensional Culture Model of Reversibly Quiescent Myogenic Cells. Stem Cells Int 2019:1–12. https://doi.org/10.1155/2019/7548160

Amirrah IN, Lokanathan Y, Zulkiflee I, et al (2022) A Comprehensive Review on Collagen Type I Development of Biomaterials for Tissue Engineering: From Biosynthesis to Bioscaffold. Biomedicines 10:2307. https://doi.org/10.3390/biomedicines10092307

Bianco S, Jangal M, Garneau D, Gévry N (2015) LRH-1 controls proliferation in breast tumor cells by regulating CDKN1A gene expression. Oncogene 34:4509–4518. https://doi.org/10.1038/onc.2014.382

Bonnans C, Chou J, Werb Z (2014) Remodelling the extracellular matrix in development and disease. Nat Rev Mol Cell Biol 15:786–801. https://doi.org/10.1038/nrm3904

Dumont NA, Wang YX, Rudnicki MA (2015) Intrinsic and extrinsic mechanisms regulating satellite cell function. Development 142:1572–1581. https://doi.org/10.1242/dev.114223

Dzamba BJ, DeSimone DW (2018) Extracellular Matrix (ECM) and the Sculpting of Embryonic Tissues. In: Current Topics in Developmental Biology. Elsevier, pp 245–274

Gilbert PM, Havenstrite KL, Magnusson KEG, et al (2010) Substrate Elasticity Regulates Skeletal Muscle Stem Cell Self-Renewal in Culture. Science 329:1078–1081. https://doi.org/10.1126/science.1191035

Hennessy N, Simms C (2023) Skeletal muscle extracellular matrix structure under applied deformation observed using second harmonic generation microscopy. Acta Biomater 172:135–146. https://doi.org/10.1016/j.actbio.2023.09.047

Khaitan D, Chandna S, Arya M, Dwarakanath B (2006) Establishment and characterization of multicellular spheroids from a human glioma cell line; Implications for tumor therapy. J Transl Med 4:12. https://doi.org/10.1186/1479-5876-4-12

Kjær M (2004) Role of Extracellular Matrix in Adaptation of Tendon and Skeletal Muscle to Mechanical Loading. Physiol Rev 84:649–698. https://doi.org/10.1152/physrev.00031.2003

Kondapaneni RV, Gurung SK, Shevde LA, Rao SS (2024) Protocol for generating dormant human brain metastatic breast cancer spheroids *in vitro*. STAR Protoc 5:102962. https://doi.org/10.1016/j.xpro.2024.102962

Motte S, Kaufman LJ (2013) Strain stiffening in collagen I networks. Biopolymers 99:35–46. https://doi.org/10.1002/bip.22133

Nicolas J, Magli S, Rabbachin L, et al (2020) 3D Extracellular Matrix Mimics: Fundamental Concepts and Role of Materials Chemistry to Influence Stem Cell Fate. Biomacromolecules 21:1968–1994. https://doi.org/10.1021/acs.biomac.0c00045

Olguín HC, Pisconti A (2012) Marking the tempo for myogenesis: Pax7 and the regulation of muscle stem cell fate decisions. J Cell Mol Med 16:1013–1025. https://doi.org/10.1111/j.1582-4934.2011.01348.x

Passaniti A, Kleinman HK, Martin GR (2022) Matrigel: history/background, uses, and future applications. J Cell Commun Signal 16:621–626. https://doi.org/10.1007/s12079-021-00643-1

Pham TL-B, Nguyen DP-H, Luu TT-T, et al (2023) Encapsulation of Human Umbilical Cord Mesenchymal Stem Cells in LunaGel Photocrosslinkable Extracellular Matrix and Subcutaneous Transplantation in Mice. Biomedicines 11:1158. https://doi.org/10.3390/biomedicines11041158

Ravi M, Paramesh V, Kaviya SR, et al (2015) 3D Cell Culture Systems: Advantages and Applications. J Cell Physiol 230:16–26. https://doi.org/10.1002/jcp.24683

Roca-Arroyo AF, Gutierrez-Rivera JA, Morton LD, Castilla-Casadiego DA (2025) Hydrogel Network Architecture Design Space: Impact on Mechanical and Viscoelastic Properties. Gels 11:588. https://doi.org/10.3390/gels11080588

Safwan-Zaiter H, Wagner N, Wagner K-D (2022) P16INK4A—More Than a Senescence Marker. Life 12:1332. https://doi.org/10.3390/life12091332

Saraswathibhatla A, Indana D, Chaudhuri O (2023) Cell–extracellular matrix mechanotransduction in 3D. Nat Rev Mol Cell Biol 24:495–516. https://doi.org/10.1038/s41580-023-00583-1

Schmittgen TD, Livak KJ (2008) Analyzing real-time PCR data by the comparative CT method. Nat Protoc 3:1101–1108. https://doi.org/10.1038/nprot.2008.73

Sun X, Kaufman PD (2018) Ki-67: more than a proliferation marker. Chromosoma 127:175–186. https://doi.org/10.1007/s00412-018-0659-8

Uxa S, Castillo-Binder P, Kohler R, et al (2021) Ki-67 gene expression. Cell Death Differ 28:3357–3370. https://doi.org/10.1038/s41418-021-00823-x

Van Santen VJB, Klein-Nulend J, Bakker AD, Jaspers RT (2022) Stiff matrices enhance myoblast proliferation, reduce differentiation, and alter the response to fluid shear stress in vitro. Cell Biochem Biophys 80:161–170. https://doi.org/10.1007/s12013-021-01050-4

Yin H, Price F, Rudnicki MA (2013) Satellite Cells and the Muscle Stem Cell Niche. Physiol Rev 93:23–67. https://doi.org/10.1152/physrev.00043.2011

Zachari MA, Chondrou PS, Pouliliou SE, et al (2013) Evaluation of The Alamarblue Assay for Adherent Cell Irradiation Experiments. Dose-Response 12:246–258. https://doi.org/10.2203/dose-response.13-024.Koukourakis

Zaman MH, Trapani LM, Sieminski AL, et al (2006) Migration of tumor cells in 3D matrices is governed by matrix stiffness along with cell-matrix adhesion and proteolysis. Proc Natl Acad Sci 103:10889–10894. https://doi.org/10.1073/pnas.0604460103

Zhang W, Liu Y, Zhang H (2021) Extracellular matrix: an important regulator of cell functions and skeletal muscle development. Cell Biosci 11:65. https://doi.org/10.1186/s13578-021-00579-4

Supplementary Files

This is a list of supplementary files associated with this preprint. Click to download.

- ESM1.pdf